A New Ultrasound Elastography Displacement Estimation Method for Mobile Telemedicine

Hong-an Li[1], Min Zhang[1], Keping Yu[2(✉)], Xin Qi[2], Li Zhen[3], Yi Gong[4,5], and Jianfeng Tong[6]

[1] College of Computer Science and Technology, Xi'an University of Science and Technology, Xi'an 710054, China

[2] Global Information and Telecommunication Institute, Waseda University, Tokyo 169-8050, Japan
keping.yu@aoni.waseda.jp

[3] School of Communications and Information Engineering, Xi'an University of Posts and Telecommunications, Xi'an 710121, China

[4] School of Information and Communication Engineering, Beijing University of Posts and Communications (BUPT), Beijing, China

[5] Global Big Data Technologies Center (GBDTC), University of Technology Sydney (UTS), Sydney, Australia

[6] School of Information Science and Technology, Northwest University, Xi'an 710127, China

Abstract. Traditional medicine requires doctors and patients to engage in face-to-face palpation, which is a great challenge in underdeveloped areas, especially in rural areas. Telemedicine provides an opportunity for patients to connect with doctors who may be thousands of miles away via mobile devices or the Internet. When using this method, elastography is a crucial medical imaging modality that maps the elastic properties of soft tissue, which can then be sent to doctors remotely. Ultrasound elastography has become a research focus because it can accurately measure soft tissue lesions. Displacement estimation is a key step in ultrasound elastography. The phase-zero search method is a popular displacement estimation method that is accurate and rapid. However, the method is ineffective when the displacement is more than a 1/4 wavelength. The block-matching method can address this shortcoming because it is suitable for large displacements, although it is not accurate. Notably, the quality-guided block matching method has exhibited good robustness under complex mutational conditions. In this paper, we propose a novel displacement estimation method that combines the block-matching method and the phase-zero search method. The block-matching method provides prior knowledge to increase the robustness of the phase-zero search under large displacement conditions. The experimental results show that our method exhibits stronger robustness, more accurate results, and faster calculation speed.

Keywords: Ultrasound elastography · Displacement estimated · Phase-zero search · Block-matching method

S. W. Loke et al. (Eds.): MONAMI 2020, LNICST 338, pp. 284–297, 2020.
https://doi.org/10.1007/978-3-030-64002-6_19

1 Introduction

In recent years, with the development of modern communication technology, telemedicine using mobile devices or the Internet has developed rapidly. This has brought great convenience to people in underdeveloped areas, even in rural areas. We can even conduct telemedicine consultations through mobile devices at home. We have seen national health authorities start to focus on E-health services such as E-health cards, electronic medical records and health portals, including the English NHS Direct Online, the German Telematics Platform, and the Danish Sundhed.dk. [1–3]. Blockchain technology is suitable for applications where independently managed biomedical/medical stakeholders (such as hospitals, suppliers, patients, and payers) wish to collaborate without ceding control to a centrally managed intermediary [4–7]. Traditional medicine relies on palpation to feel the size, shape or firmness of soft tissue, but this technique cannot provide accurate or concrete analysis. The firmness of biological soft tissue can provide important evidence for the early diagnosis of a nidus, especially for the diagnosis of tumors [8]. Ophir J. proposed the ultrasonic elastography method [9, 10], which is different from the traditional ultrasonic imaging method in that it can reflect the physical information of soft tissue through images, such as the Young's modulus. However, the traditional ultrasound imaging method provides only a reflection of the acoustic impedance of soft tissue. The conventional ultrasound imaging method has a limited ability to distinguish soft tissues with small differences in acoustic impedance, and it is prone to interference from various factors in the detection of deeper tissues of the body. Ultrasound elastography technology can address this deficiency. Ultrasound elastography has become a research topic of interest in the field of ultrasonic imagery both at home and abroad, and various improved ultrasonic imaging methods have emerged, such as O'Donnell M.'s envelope cross-correlation method [11], Sarvazyan A.P.'s method of shear wave elastography [12], Fatemi M.'s acoustic radiation imaging method [13], Varghese T.'s time-domain stretching method [14], and Sarvazyan A. P.'s alternating strain estimation method [15].

Using Ophir J.'s method, we can create a slight deformation of the tissue (1% to 2%) by applying a little pressure and collect an ultrasonic signal before and after the procedure through an ultrasonic device. Using a time-domain cross-correlation to compare the two sets of signals, we can obtain the displacement of each point in the tissue and calculate the displacement difference to obtain the tissue strain; the reciprocal of the strain is used to appropriately represent the physical attributes of the tissue. Although we cannot quantitatively measure the tissue elasticity with Ophir J.'s method, we can clearly distinguish tissues with different hardness levels. The accuracy of time-domain cross-correlation is subject to the ultrasonic frequency, the sampling rate and the signal-to-noise ratio and is more sensitive to the sampling rate when the signal-to-noise ratio is high.

In O'Donnell M.'s method, the signal envelope cross-correlation method is used to calculate the tissue displacement [11]. In this method, a Hilbert transform is performed on the collected RF to obtain the analytical signal, and the analytical signal is cross-correlated. By analyzing the phase of the analytical signal cross-correlation function, the displacement data of the tissue can be obtained. Due to the periodic characteristics of the phase, this method can only be used when the maximum displacement is less than a 1/4

wavelength. When the displacement is greater than a 1/4 wavelength, phase cancellation will occur and produce an incorrect displacement. To circumvent this limitation, Shiina T. proposed a CAM (Combined Autocorrelation Method) [16, 17], which expanded the application scope of the method. However, the CAM requires a large amount of computation and is greatly affected by noise.

The block-matching method is widely used in video compression and video tracking applications [18]. It divides the target frame into blocks of the same size. For each block, the best matching position is found in the reference frame (usually the adjacent frame of the target frame). There are many measures of matching degree, including SAD (Sum of Absolute Differences), MSD (Mean Square Differences) and NCC (Normalized Cross Correlation). The best matching location search methods include FS (Full Search), TSS (Three-Step Search), NTSS (New Three-Step Search), and 4SS (Four-Step Search) [19]. To narrow the search scope, the search can be carried out around the best matching position that has been calculated for the adjacent blocks. However, because this search method based on prior knowledge, it can lead to error accumulation and obtain intolerable error results. In this paper, a quality-guided block matching method is adopted to improve the computing speed and avoid the accumulation of errors.

In this paper, we take advantage of the technical merits of the quality-guided block matching method and the phase-zero search method. We combine these two popular methods into our new method to estimate the tissue displacement, achieving good experimental results. The structure of this paper is organized as follows. Section 1 introduces the current research background of ultrasound elastography in the E-health field. Section 2 presents the quality-guided block matching method and the phase-zero search method, and our algorithm framework is outlined. The experiments and analysis are presented in Sect. 3, and we compare our proposed model with two popular methods. Section 4 concludes this paper.

2 Algorithm Framework

2.1 Quality-Guided Block Matching

In our method, we take the sum of absolute differences (SAD) as the measurement of matching degree, and it is defined as follows:

$$SAD = \sum_{i=1}^{m} \sum_{j=1}^{n} |A(i,j) - B(i,j)| \tag{1}$$

where $m \times n$ is the size of the block, A is the block to be computed in the target frame and B is the block of the reference frame. Corresponding to the reference frames, the best matchable position in block $A(k, s)$ is:

$$B(k+p', s+q') = \arg\min\left(\sum_{i=k}^{k+m} \sum_{j=s}^{s+n} |A(i,j) - B(i+p, j+q)| | p \in (-a, a), q \in (-b, b)\right) \tag{2}$$

where $(-a, a)$ is the transverse searching scope and $(-b, b)$ is the vertical searching scope. Meanwhile, we take the displacement of the points in block A as a vector (p', q'). On the basis of the traditional block searchin, which computes the displacement of every block by either row order or column order, using the result of the neighboring block of the current block as a reference computes the displacement of the current block. Due to the effect of noise, errors can accumulate continuously and even result in a large error if there is a displacement error in one block.

The quality-guided block matching method [20] does not calculate the blocks in the target frame in the order of row and column; it calculates the displacement of its neighbor block by referring to the block with the highest matching degree at a given point in time. Using this method can ensure that the more matchable block gets calculated first, and the block that has more noise and easily results in error is computed last, thus avoiding the transmission and accumulation of errors. The steps of this method are as follows:

Step 1. Select the starting block A and put it into the set S to calculate the displacement and matching degree of block A;
Step 2. Find the most matchable block in set S and take it as the current block. If there is more than one candidate, then randomly select from the candidates;
Step 3. Compute the displacement and matching degree of the current block;
Step 4. If there are neighboring blocks of the current block that have not been computed, go to Step 5; otherwise, go to Step 7;
Step 5. If the neighboring block chosen in the last step was not in set S, initialize the neighboring block with the displacement and matching degree of the current block, put it into set S and go to Step 4. If it was in set S, go to Step 6;
Step 6. If the matching degree of neighboring block is higher than the current block, go to Step 4; otherwise, update the displacement and matching degree of the neighboring block with that of the current block and go to Step 4;
Step 7. Remove the current block from set S;
Step 8. If set S is not empty, go to Step 2, otherwise the steps are finished.

2.2 Phase-Zero Search

The phase-zero search first calculates the analytical form of the two frames of signals before and after palpation, and then, it calculates the position of the phase-zero crossing by using the cross-correlation of the analytical signals, i.e., the position of the maximum value of the cross-correlation function.

The bandpass of the two signals $x_1(t)$ and $x_2(t)$ are described as:

$$\tilde{x}_1 = A(t - \tau_1)e^{-i\omega_0\tau_1},\ \tilde{x}_2 = A(t - \tau_2)e^{-i\omega_0\tau_2} \tag{3}$$

The complex cross-correlation functions of the two signals are described as:

$$\tilde{C}(t) = \frac{1}{T}\int_0^T \tilde{x}_1(\tau)\tilde{x}_2^*(t + \tau)d\tau \tag{4}$$

When t is 0, we can obtain the simplified form of the above expression:

$$\tilde{C}(0) = \Gamma_{AA}(\tau)e^{i\omega_0\tau} \tag{5}$$

where $\Gamma_{AA}(\tau)$ is an autocorrelation function of the signal envelope. The time delay of signals $x_1(t)$ and $x_2(t)$ can be described with the above phase-zero search:

$$\tau_{\mathrm{BB}} = \frac{\phi(0)}{\omega_0} = \frac{\tan^{-1}(\frac{\mathrm{Im}(\tilde{C}(0))}{\mathrm{Re}(\tilde{C}(0))})}{\omega_0} \tag{6}$$

The displacement is:

$$d = \tau_{BB} \cdot c \tag{7}$$

where c is the ultrasonic propagation velocity in the medium.

This method can obtain equal accuracy with oversampling by a lower calculation and cause phase cancellation, resulting in a miscalculation of time delay when the displacement is more than a half phase. Combining block-matching with a phase-zero search can obtain an accurate displacement field after first computing a rough displacement with block-matching that limits the error no more than a half phase. To clearly reflect the physical characteristic of the tissue, we compute the strain field from the displacement field with the gradient method. The algorithm framework is as follows (Fig. 1):

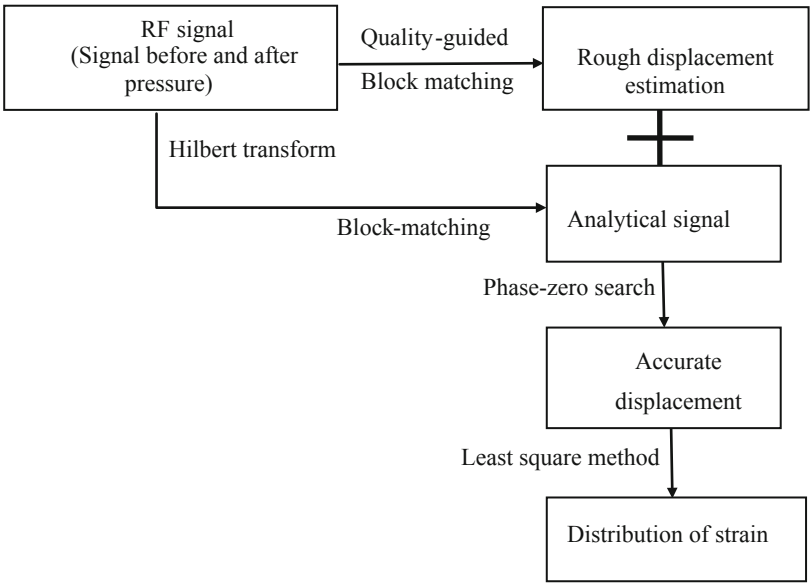

Fig. 1. The algorithm framework

3 Experiment and Analysis

A two-dimensional soft tissue model was created using Abaqus software, and this model contained circular tissue that was four times harder than the surrounding tissue. Then,

a 2% deformation is generated in the model, and a simulated RF signal is generated by the consistent displacement generated by the deformation. In this set of simulation data, the central frequency of the signal is 5 MHz, the sampling rate is 20 MHz, and the maximum displacement is greater than twice the length of the ultrasonic wave. The CAM [16, 17] and the traditional TDE (Time Delay Estimation) algorithm [21] are classical and popular methods of the current displacement estimation methods. Therefore, this paper uses these methods as a comparative experiment.

3.1 Combined Autocorrelation Method

To maintain simplicity, we consider only the axial displacement of the tissue (that is, along the direction of the beam). Supposing that the signal distortion caused by tissue deformation (the decorrelation of speckle structure) is locally ignored, the RF signal measured before and after distortion can be modeled as

$$\begin{aligned} x(t) &= u(t)e^{-j(\omega_0 t-\theta)} \\ y(t) &= u(t-\tau)e^{-j[\omega_0(t-\tau)-\theta]} \end{aligned} \tag{8}$$

where they are complex expressions and u, ω_0 and τ represent the envelope, the carrier angular frequency and the time shift, respectively. We define the complex cross-correlation function between $x(t)$ and $y(t + nT/2)$ as

$$\begin{aligned} R_{xy}(t;n) &= \int_{-t_0/2}^{t_0} x(t+v)y(t+nT/2+v) * dv \\ &= R_u(t;\tau - nT/2)e^{-j\omega_0(\tau-nT/2)} \\ &(n = \ldots -2, -1, 0, 1, 2\ldots) \end{aligned} \tag{9}$$

where T is an ultrasonic period and $R_u(t;\tau)$ represents the autocorrelation function of the envelope. For the special case of, $n = 0$ Eq. 9 becomes:

$$R_{xy}(t;0) = \int_{-t_0/2}^{t_0/2} x(t+v)y(t+v) * dv = R_u(t;\tau)e^{-j\omega_0\tau} \tag{10}$$

This expression corresponds to the output of the autocorrelation operator of a traditional Doppler system. The difference is that the Doppler method uses a moving average filter instead of averaging the subsequent sequence. If the displacement δ is less than a quarter of the wave length, the displacement can be obtained by the phase shift $\phi = \omega_0\tau$:

$$\delta(t) = \frac{\phi}{2\pi}\lambda = \frac{\omega_0\tau}{2\pi}\lambda \tag{11}$$

It is impossible to estimate δ unambiguously from Eq. 10 except by using a priori knowledge about displacement or the standard simple form of expansion (only extending the aliasing limit from $\lambda/4$ to $\lambda/2$).

To avoid fuzziness, the envelope correlation coefficient $C_u(t;n)$ defined by Eq. 12 is adopted, but it also brings a certain amount of calculation.

$$C_u(t;n) = \frac{\left|R_{xy}(t;n)\right|}{|x(t)||y(t+nT/2)|} \tag{12}$$

According to Eqs. 9 and 12, the two sets C_u and ϕ can be obtained for every time t:

$$\{C_u(t)\} = \left\{C_u^{-M}, \ldots, C_u^{-1}, C_u^0, C_u^1, \ldots, C_u^N\right\}$$
$$\{\phi(t)\} = \{\phi^{-M}, \ldots, \phi^{-1}, \phi^0, \phi^1, \ldots, \phi^n\} \tag{13}$$

where $C_u^n = C_u(t; n)$ and ϕ^n is the phase of $R_{xy}(t; n)$. If M and N are designated large enough, a component of $\{\phi(t)\}$, ϕ^k will not be wrapped because if it comes from the two sequences $x(t)$ and $y(t + kT/2)$, the displacement t between the two sequences is less than $\lambda/4$. Meanwhile, C_u^n becomes the maximum at $n = k$. Therefore, the first step is to determine the maximum value of C_u^n at n, after which the unwrapped phase shift can be obtained as $\phi(n) = \arctan(R_{xy}(n))$, and the displacement δ can be calculated from Eq. 11. Finally, the strain along the beam direction $s(t)$ can be calculated as follows:

$$s(t) = \frac{d\delta}{dt} \tag{14}$$

From the perspective of envelope correlation, the first step is similar to the speckle tracing algorithm. The first and second steps can occur simultaneously through autocorrelation processing, and C_u is computed only a few times; that is, $N + M + I$ determines the unwrapped region. So the processing speed is faster than the speckle tracking, and the correlation coefficient is calculated by changing τ many times.

In practice, as shown in Fig. 2, by using multiple autocorrelation processing units in parallel, it should be possible to perform real-time processing similar to traditional Doppler methods.

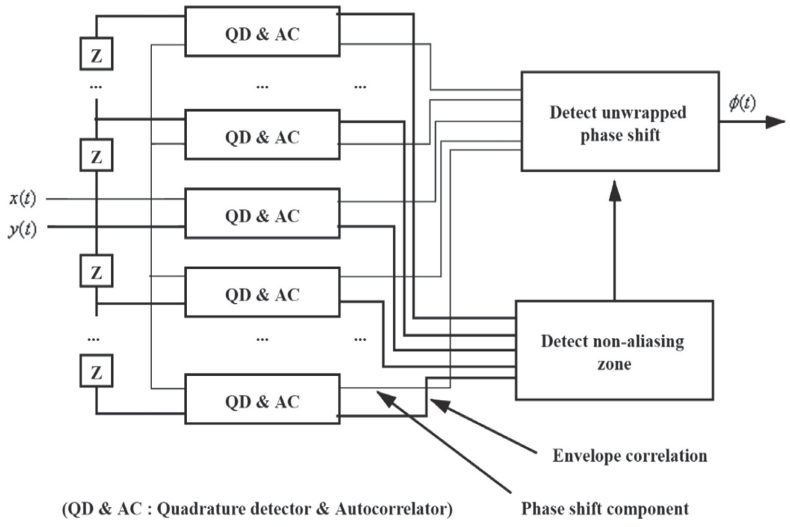

Fig. 2. Combined autocorrelation method

3.2 Time Delay Estimation

Time delay estimation is used to calculate the time delay of a reference signal and a contrast signal in a period of time. As shown in Fig. 3, the time shift exists between the reference signal and the contrast signal. The present TDE method has good performance under high Signal to Noise Ratio (SNR). However, with the decrease of signal correlation, the performance decreases, so the robustness is poor.

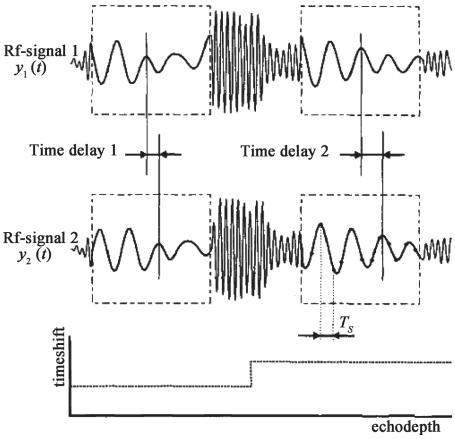

Fig. 3. Reference signal and delay signal

Because the tissue vibration is small and its orders of magnitude are usually measured in microns, the sampling frequency of common ultrasonic equipment cannot meet the requirement. Therefore, a signal interpolation algorithm must be used to improve the estimation accuracy of displacement. The interpolation algorithm is an important function approximation method. The spline interpolation finds a set of fitting polynomials according to the existing data points. In the fitting process, a polynomial is used to fit the curves for adjacent data points, which is mostly used in signal processing.

In signal processing, the mutual transformation of continuous and discrete signals is a basic task, and the spline interpolation is the most suitable method. Schoenberg proposed the theoretical basis of spline interpolation and introduced the B-spline curve. Spline curves are represented by piecewise polynomials and connected together smoothly. Connection points are called nodes. For an n-order spline interpolation, each segment of its polynomial is an n-order, and each segment of the curve requires $n+1$ coefficients. The curvature of a cubic spline curve is the smallest, so it is mostly used in practice.

Let Δ be a division of $[a, b]$, $\Delta \cdot a = x_0 < x_1 < \cdots < x_n = b$. If $S(x)$ satisfies:

a. $S(x) \in C^2[a, b]$;
b. $S(x_i) = f(x_i), i = 0, 1, 2, 3, 4$;
c. $S(x)$ is a polynomial of degree no greater than three in all subintervals and is a polynomial of degree of at least one subinterval; then $S(x)$ is a cubic spline function that divides Δ.

The cubic spline interpolation is typically used in signal processing because of the balance between computation and accuracy. With spline interpolation, the discrete signal can be expressed in a continuous form as a polynomial. Then, the original signal can be interpolated by increasing the sampling frequency or by directly applying the polynomial coefficient to the delay calculation.

The cubic spline is a piecewise cubic polynomial, and the first and second derivatives of the node are continuous. The sampling result of signal $r(i\Delta t)$ can be expressed as

$$r(i\Delta t) = p_i(t) = a_1 t^3 + b_1 t^2 + c_i t + d_i \tag{15}$$

The third-order interpolation of the original data can obtain a balance between performance and computation. The interpolation effect at a third order and above cannot be optimized; the error increases and the computational efficiency decreases.

Let the reference signal and the contrast signal be $x_1(n)$ and $x_2(n)$ respectively; the expressions are as follows:

$$x_1(n) = s(n) + v_1(n),\ x_2(n) = s(n) + v_2(n) \tag{16}$$

The correlation function of the two signals is

$$R_{12}(\tau) = |E(x_1(n)x_2(n-\tau))| = R_{ss}(\tau - D) + R_{sv_1}(\tau - D) + R_{sv_2}(\tau) + R_{v_1 v_2}(\tau) \tag{17}$$

where $v_1(n)$ and $v_2(n)$ are noises; D is the time difference of reaching the sensor. In engineering, the noise is independent of the signal, that is,

$$R_{12}(\tau) = Rss(\tau - D) \tag{18}$$

From the properties of related functions, the function reaches the maximum value at $\tau = D$:

$$D = \arg\{\max[Rss(\tau - D)]\} \tag{19}$$

where arg represents the independent variable of the function; max denotes the maximum value of the function. The estimated value of D is obtained from the above equation when the cross-correlation function is maximized. Based on this theory, the time-domain cross-correlation is used to estimate the vibration displacement of the organization.

$$R(\tau) = \frac{\sum_{i=0}^{T-1} s_1(\tau)s_2(\tau + i)}{\sqrt{\sum_{k=0}^{T-1} [s_1(\tau + k)]^2 \sum_{j=0}^{T-1} [s_2(\tau + j)]^2}} \tag{20}$$

where S_1 is the reference RF signal; S_2 is the signal after vibration; T is the window size in the time domain; τ is the axial time point, and the range of τ is determined by the longitudinal length of radio frequency echo data and the prior knowledge of compression. This formula can be used to calculate the cross-correlation peak of the two segments before and after compression, so the displacement of the tissues before and after compression at different depths can be obtained by the offset of the cross-correlation peak along the time axis.

3.3 Estimation of Longitudinal Displacement

In the TDE method, RF signals are initially oversampled. When looking for the peak of the cross-correlation function, the parabolic interpolation method is adopted. Figures 4 (a), (b) and (c) show the displacement field calculated by the TDE method, the CAM method and our method, respectively, and Fig. 4 (d) shows the comparison between the displacement distribution of the three methods on a longitudinal line and the real displacement distribution.

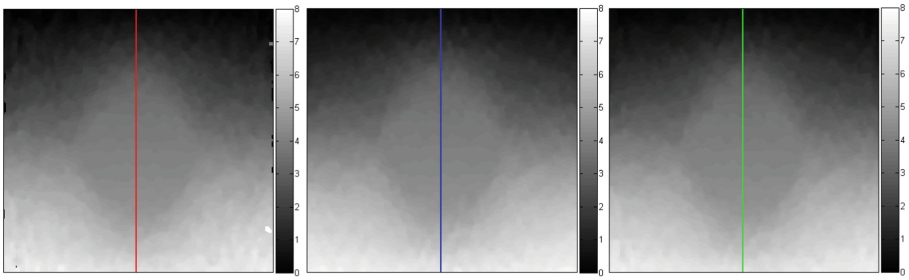

(a) TDE (b) CAM (c) Ours

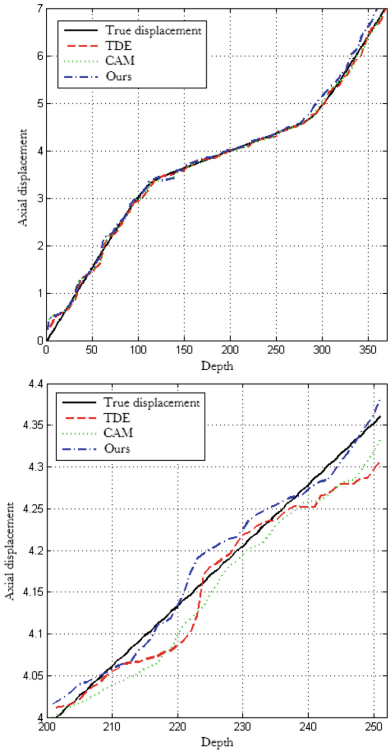

(d) Displacement distribution in one line

Fig. 4. Displacement calculation comparison of three methods

It can be seen that the method in this paper is closer to the real displacement distribution because the method in this paper takes the displacement of the neighboring points as the prior information when calculating the displacement of a certain point, which not only improves the accuracy but also greatly reduces the search scope, thus reducing the amount of calculation and speeding up the calculation speed. To obtain the same result as the method in this paper, the TDE method needs to carry out oversampling with a very large amount of computation. There are also many redundant cross-correlation calculations in the CAM method, and the half wavelength limitation cannot be broken. To quantitatively analyze the accuracy of the three methods, we define the displacement difference of the calculation results as:

$$\sigma = \sqrt{\frac{\sum_{i=1}^{n} (result_i - true_i)^2}{n}} \tag{21}$$

where *result* is the displacement field calculated, and *true* is the error of the three methods, n is the number of samples. These results are shown in Table 1, which are 0.1156, 0.0798 and 0.0657, respectively. Obviously, the Displacement field error of this method is the smallest, which indicated that the calculation result of this method is more accurate. This is shown in Fig. 4, the method in this paper is closer to the real displacement distribution.

Table 1. Three methods of displacement field error

Method	TDE	CAM	Ours
Displacement field error	0.1156	0.0798	0.0657

3.4 Strain Estimation

To clearly indicate the physical characteristic of the tissue, we compute the tissue strain on the basis of the gained displacement field with the least square method, namely, the tissue strain is represented by a gradient. Figures 5 (a), (b), (c) separately represent the results of the TDE, the CAM and the method in this paper. As seen from the figure, the result obtained by the method in this paper is smoother, and the diseased tissue is easier to distinguish. Figure 5 (d) shows the strain distribution at the midline position.

A comparative transport rate (CNR) is adopted to quantitatively analyze the lesion degree resolution of the tissue of each method:

$$CNR = \frac{m_b - m_t}{\sqrt{(\sigma_b^2 + \sigma_t^2)/2}} \tag{22}$$

where m_b, σ_b are the mean and standard deviation of the background, and m_t, σ_t are the mean and standard deviation of the target. These are shown in Table 2. The CNRs of the three methods are calculated as follows: 7.67, 26.08, 157.06. Obviously, after comparison, the CNR of our method is the highest, which is the same as that shown in Fig. 5.

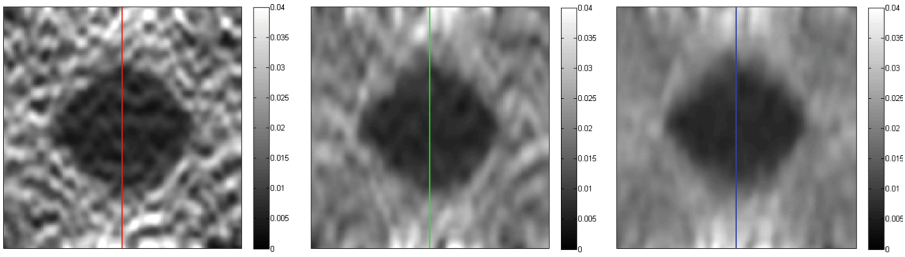

(a) TDE (b) CAM (c) Ours

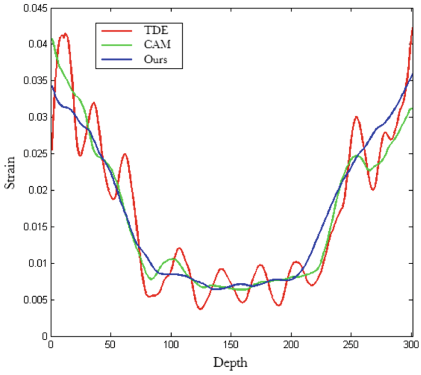

(d) Displacement distribution in one line

Fig. 5. Strain comparison of three methods

Table 2. Three methods of comparative transport rate

Method	TDE	CAM	Ours
CNR	7.67	26.08	157.06

4 Conclusion

This paper presents a new displacement estimation method for ultrasound elastography, namely, the QGBM + PS method. The experimental results show that this method can accurately and efficiently calculate the displacement field and effectively solve the error transmission problem when using prior information. In the future, this method will be further optimized. For example, in the QGBM method, the determination of block size can be adaptive. In the PS method, the results can be calculated by an iterative method to make the results more accurate. In addition, a GPU array can be used to accelerate the method to meet real-time requirements [22, 23]. With the development of modern communication technology, telemedicine using mobile devices or the Internet will become more popular.

Acknowledgments. This work was supported in part by the Natural Science Basic Research Plan in Shaanxi Province of China (2019JM-162), and in part by the Japan Society for the Promotion of Science (JSPS) Grants-in-Aid for Scientific Research (KAKENHI) under Grant JP18K18044.

References

1. Andreassen, H.K., Bujnowska-Fedak, M.M., Chronaki, C.E., et al.: European citizens use of E-health services: a study of seven countries. BMC Public Health **7**(53), 1–7 (2007)
2. Hongan, L., Min, Z., Keping, Y., et al.: Combined forecasting model of cloud computing resource load for energy-efficient IoT system. IEEE Access **7**, 149542–149553 (2019)
3. Liu, Z., Dong, M., Gu, B., et al.: Fast-start video delivery in future internet architectures with intra-domain caching. Mob. Netw. Appl. **22**(1), 98–112 (2017)
4. Kuo, T.T., Hsu, C.N., Ohno-Machado, L.: Model chain: decentralized privacy-preserving healthcare predictive modeling framework on private block chain networks, pp. 1–13 (2016). https://www.healthit.gov/sites/default/files/10-30-ucsd-dbmi-onc-blockchain-challenge.pdf
5. Liu, Z., Feng, J., Ji, Y., et al.: EAF: energy-aware adaptive free viewpoint video wireless transmission. J. Netw. Comput. Appl. **46**, 384–394 (2014)
6. Hongan, L., ZhuoMing, D., Jing, Z., Zhanli, L.: A retrieval method of medical 3D models based on sparse representation. J. Med. Imaging Health Inf. **9**(9), 1988–1992 (2019)
7. Kuo, T.T., Kim, H.E., Ohno-Machado, L.: Blockchain distributed ledger technologies for biomedical and health care applications. J. Am. Med. Inform. Assoc. **24**(6), 1211–1220 (2017)
8. Yan, F., Song, Z., Du, M., Klibanov, A.L.: Ultrasound molecular imaging for differentiation of benign and malignant tumors in patients. Quant. Imaging Med. Surg. **8**(11), 1078–1083 (2018)
9. Gennisson, J.L., Deffieux, T., Fink, M., et al.: Ultrasound elastography: principles and techniques. Diagn. Interv. Imaging **94**(5), 487–495 (2013)
10. Ophir, J., Cespedes, I., Ponnekanti, H., et al.: Elastography: a quantitative method for imaging the elasticity of biological tissues. Ultrason. Imaging **13**(2), 111–134 (1991)
11. O'Donnell, M., Skovoroda, A.R., Shapo, B.M., et al.: Internal displacement and strain imaging using ultrasonic speckle tracking. IEEE Trans. Ultrason. Ferroelectr. Freq. Control **41**(3), 314–325 (1994)
12. Sarvazyan, A.P., Rudenko, O.V., Swanson, S.D., et al.: Shear wave elasticity imaging: a new ultrasonic technology of medical diagnostics. Ultrasound Med. Biol. **24**(9), 1419–1435 (1998)
13. Fatemi, M., Greenleaf, J.F.: Ultrasound-stimulated vibro-acoustic spectrography. Science **280**(5360), 82–85 (1998)
14. Varghese, T., Ophir, J.: Enhancement of echo-signal correlation in elastography using temporal stretching. IEEE Trans. Ultrason. Ferroelectr. Freq. Control **44**(1), 173–180 (1997)
15. Sarvazyan, A.P.: A new approach to remote ultrasonic evaluation of viscoelastic properties of tissues for diagnostics and healing monitoring. In: Abstract of ARPA/ONR Medical Ultrasonic Imaging Technology Workshop 1, pp. 24–26 (1995)
16. Shiina, T., Doyley, M.M., Bamer, J.C.: Strain imaging using combined RF and envelope autocorrelation processing. In: Ultrasonics Symposium 2, pp. 1331–1336 (1996)
17. Shiina, T., Yamakawa, M., Nitta, N., et al.: Clinical assessment of real-time, freehand elasticity imaging system based on the combined autocorrelation method. In: IEEE Symposium on Ultrasonics, Honolulu, USA, pp. 664–667 (2003)
18. Gyaourova, A., Kamath, C., Cheung, S.C.: Block matching for object tracking. Department of Computer Science, University of Nevada, Reno, pp. 1–15 (2003)
19. Nie, Y., Ma, K.K.: Adaptive rood pattern search for fast block-matching motion estimation. IEEE Trans. Image Process. **11**(12), 1442–1449 (2002)

20. Chen, L., Treece, G.M., Lindop, J.E., et al.: A quality-guided displacement tracking algorithm for ultrasonic elasticity imaging. Med. Image Anal. **13**(2), 286–296 (2009)
21. Ke, C., Jiangli, L., Guanxiong, H.: Tissue motion estimation based on ultrasound RF signal and TDE algorithm. J. Xihua Univ. (Nat. Sci. Ed.) **36**(4), 1–4 (2017)
22. Liu, Z., Cheung, G., Ji, Y.: Optimizing distributed source coding for interactive multiview video streaming over lossy networks. IEEE Trans. Circuits Syst. Video Technol. **23**(10), 1781–1794 (2013)
23. Qingfang, L., Baosheng, K., Keping, Y., Xin, Q., Jing, L., Shoujin, W., Hongan, L.: Contour-maintaining-based image adaption for an efficient ambulance service in intelligent transportation systems. IEEE Access **8**, 12644–12654 (2020)